2001 IEEE Inernational Ultrasonics Symposium
Atlanta, USA, Oct. 7-10, 2001, pp. 541-544

OPTIMIZATION OF A BULK-DRIVEN SURFACE MICROMACHINED ULTRASONIC MICROMOTOR

Ville Kaajakari and Amit Lal
*Sonic*MEMS Laboratory, Department of Electrical and Computer Engineering
University of Wisconsin-Madison, 1415 Engineering Drive, Madison, WI 53706, USA

Abstract – This paper reports on performance and optimization of an ultrasonically driven surface micromachined motor. The rotor thickness and diameter are 2.5 μm and 1000 μm respectively, and is actuated by a piezoelectric PZT (lead-zirconate-titanate) plate with segmented electrodes. The motor operates with sub-three volt peak-to-peak excitation in atmospheric pressure. Parametric excitation of a plate in conjuction with mode splitting is observed on the stator hub resulting in traveling modes with vibration amplitude of approximately 1 μm. The rotation direction can be controlled by selectively exciting different electrodes on the PZT plate. The piezoelectric plate is adhesively mounted to silicon die after the surface micromachine fabrication making the method suitable for actuating micromachines from any surface micromachine process.

I. INTRODUCTION

Macro scale ultrasonic motors have been used in applications like auto-focus cameras requiring small form [1]. Compared to the conventional electromagnetic motors, ultrasonic motors have a large torque-to-speed ratio eliminating the need for gear reduction. They also have a large hold-on torque without requiring energy consumption. Ultrasonic actuation is based on frictional coupling [1] or acoustic streaming [2] of vibrations from a piezoelectrically actuated stator to a rotor. Since the rotor/stator do not have to be conductive, a wider choice of rotor/stator material is possible, as compared to the electrostatic, magnetic, or thermally driven actuators.

There have been previous attempts in fabricating micromachined ultrasonic motors. Moroney *et al.* reported on ultrasonic actuation of polysilicon particles using flexural plate waves (FPWs) on silicon nitride membranes [3]. Flynn *et al.* also recognized the advantages of piezoelectric materials for microrotor actuation [4]. The devices by Flynn *et al.* consisted of a bulk micromachined nitride membrane actuated by a sol-gel PZT (lead-zirconate-titanate) thin film. The rotor was not integrated in the fabrication process but was manually placed on the nitride membrane. Also, special processing of piezoelectric film can be costly and occasionally conflicts with cleanliness requirements of an IC fabrication facility making batch fabrication difficult.

At MEMS 2000 we presented initial results on the surface micromachined motor driven by piezoelectric pulses [5]. However, the control of rotation direction originated from packaging-related boundary conditions, which is undesirable from system design perspective. In addition to demonstrating rotation direction control with segmented PZT electrodes, we present here new results on analytical modeling, torque measurements, nonlinear hub excitation, and optimization of the PZT/Si laminate.

II. DEVICE FABRICATION

The rotor was fabricated using the SUMMiT-IV polysilicon surface micromachining process [6]. The rotor thickness and diameter are 2.5 μm and 1000 μm respectively making it to authors' knowledge the smallest ultrasonic motor. After release and critical point drying a rectangular PZT4 (lead-zirconate-titanate) plate (4 mm·4 mm·0.3 mm) was mounted on the back of the die using cyanoacrylate adhesive (Figure 1). The relatively large PZT area as compared to rotor size was to facilitate easy handling. The PZT plate electrodes were segmented for rotation direction control and contact wires were soldered on the corners of the PZT plate.

III. PZT/SI LAMINATE EXCITATION

The actuation is based on exciting traveling waves on the hub. The hub resonances are excited by driving the PZT/Si composite show in Figure 2 at or near the hub resonant frequency. Rotating modes couple momentum to the rotor resulting in continuous motor rotation. The hub acts as a micromotor stator. Both standing and rotating hub resonant modes are observed with phase-locked interferometer imaging system when the composite is driven in vacuum.

While quantitative modeling of the PZT/Si-laminate vibrations requires 3D FEM simulation, qualitative agreement with measured impedance can be obtained with 1D

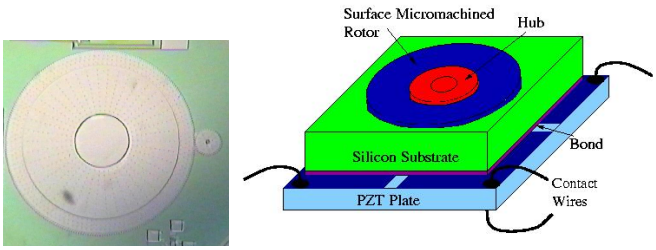

Figure 1. *A photo of the rotor and PZT plate actuation schematic. The PZT electrodes have four segments.*

model as shown in Figure 3 showing the measured and calculated PZT impedance. The material properties used in simulation are given in Table 1. Using the 1D model, it is possible to optimize PZT thickness given silicon and adhesive thickness. Figure 4 shows the silicon surface displacement and surface velocity versus PZT thickness for fixed actuation voltage. Increasing PZT thickness also increases the electrical impedance and thus reduces the power consumption. Using these design guidelines, the PZT thickness was increased from 380 μm to 500 μm resulting in threshold actuation voltage over the PZT dropping from 4.5 V_{PP} to 2.4 V_{PP} and power consumption decreasing from approximately 15 mW to 3 mW in atmospheric pressure. The power consumption can be reduced further by decreasing the PZT area.

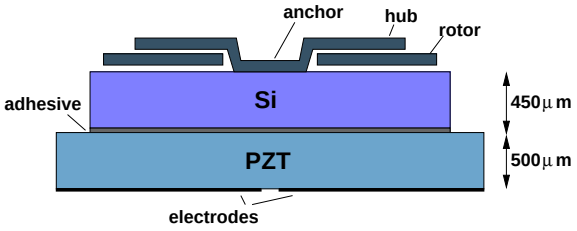

Figure 2. *PZT/Si laminate with hub and rotor*

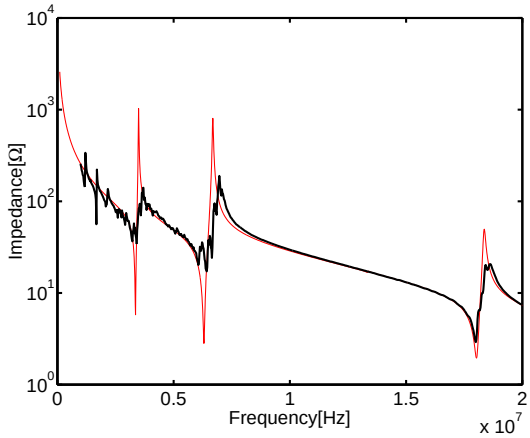

Figure 3. *Measured and simulated electrical impedance for PZT/silicon laminate.*

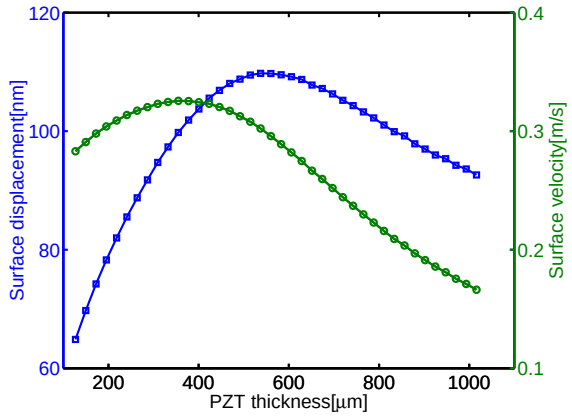

Figure 4. *Simulated silicon surface displacement and velocity vs. PZT thickness.*

Table 1. *Material properties used for the simulations*

	$c_{33}^D[GPa]$	ρ[kg/m^3]	Q	e[C/m^2]	$\varepsilon/\varepsilon_0$
PZT^a	159	7500	168	15.2	667.6
PZT^b	159	7500	500	15.1	635
Glue^a	10.7	1010	30		
Glue^b	10.2	1070			
Si^a	190	2300	200		
Si^b	190	2300			

^{a} Values used for simulations giving the best the least-square fit
^{b} Published values [7, 8]

IV. Hub mode excitation

The PZT/Si-laminate vibrations can couple to the surface micromachines via stress or inertial coupling. For stress coupling, the substrate stresses couple to the surface micromachines through the surface micromachine anchor. For inertial coupling, the moving substrate surface with acceleration $\ddot{u}$ exerts force $F = m\ddot{u}$ on the surface micromachines with mass m. The placement of the microstructure effects the coupling mechanism.

Mode splitting

If the substrate is excited near the hub resonance, the hub can vibrate with vibration amplitude of several hundreds of nanometers and the vibrations into nonlinear regime. Moreover, in our experiments we observe rotating (traveling) vibration modes with single source excitation. The classical plate theory assumes that the disk is perfect and the natural modes have no angular preference. For ideal plate, there are two angular solutions $\Theta_1 = \cos(n\theta)$ and $\Theta_2 = \sin(n\theta)$. The solutions are degenerate having exactly the same natural frequency. The ideal plate theory cannot explain rotating modes for single frequency and single source excitation.

In all practical plates there are alway some imperfections. Zenneck [9] showed that these imperfections cause the degenerate (Θ_1 and Θ_2) angular solutions to split in frequency and obtain angular preference orthogonal to each other. A typical anchored plate used in the experiments is shown in Figure 5. For fabrication purposes, it has etch holes placed periodically to reduce the release etch time. These etch holes cause the vibration modes to split. The mode that has the nodes at etch holes, has higher effective mass than the mode with holes and anti-nodes coinciding. If both modes are excited, their sum in general is a combination of standing and rotating waves. Since the modes have almost the same natural frequency, both modes can be excited with a single frequency source. Moreover, the rotation direction of the combined mode can be controlled by varying the excitation point and thus changing the relative phases of the modes.

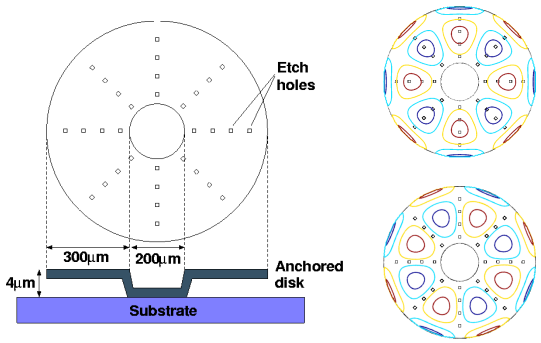

Figure 5. *A schematic of the anchored disk with two preferred orientations for the $R_{4,1}$-mode.*

Hub vibration measurements

The hub displacement was measured with a laser Doppler interferometer (Polytec PI). Figure 6(a) shows the displacement at 2 V_{PP} excitation at 3.85 MHz in atmospheric pressure. The excitation source impedance was 50 Ω and thus the actual voltage over PZT was lower (∼1.3 V_{PP}). The vibration amplitude is 1.3 nm at the excitation frequency measured at a point approximately 100 μm inside the hub edge. The edge vibration amplitude is approximately twice as large. Figure 6(b) shows the displacement for the same sample at 3 V_{PP}. The vibration amplitude is now two orders magnitude higher (250 nm) and the vibration is split into two modes around 1.9 MHz. The substrate displacement was approximately 2 nm giving amplification factor of 125. The parametric excitation is believed to be due to non-linearities in the large amplitude plate vibrations. The sum of the two excited modes can result in mixed standing and rotating mode, thus explaining the rotor rotation. The large vibration amplitude suggests that the hub rotor coupling is due to direct contact between the hub and rotor. This is further confirmed by vibration measurements at 4 V_{PP} showing clipping in vibration amplitude due to hub-rotor impacts (Figure 7). It is quite remarkable that micrometer vibrations are obtained in atmospheric pressure where surface micromachine vibrations are typically heavily damped.

Stator/rotor coupling

The large amplitude hub vibrations cause the rotor and stator to be in direct contact at the edge of the stator where the vibration amplitude is the largest. For a pure rotating mode, the hub displacement is

$$w(r,\theta,t) = AR_{n,m}(r)\cos(n\theta - \omega t), \qquad (1)$$

where A is amplitude and $R_{n,m}(r)$ is the radial solution. If there is no sliding between the rotor and the stator, the rotor angular velocity is [10]

$$\dot{\theta}_{rotor} = -A\omega\frac{nh}{2r_0^2}R(r_0). \qquad (2)$$

The rotor is driven in the opposite direction than the traveling wave. An estimate of the expected rotor velocity is then obtained by substituting $AR(r_0) = 1$ μm,

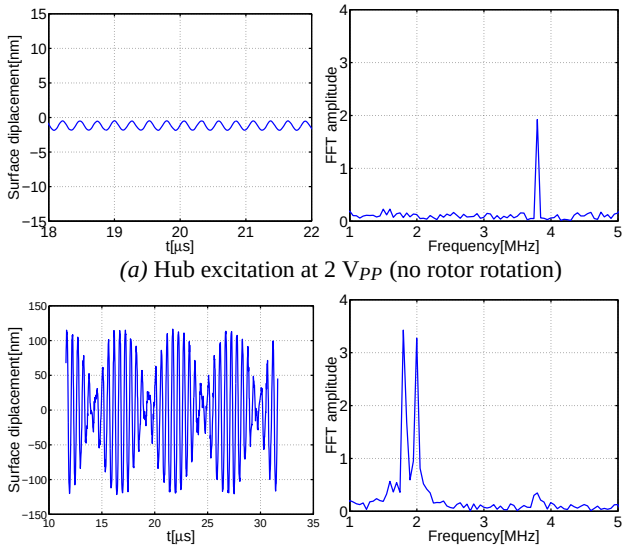

(a) Hub excitation at 2 V_{PP} (no rotor rotation)

(b) Hub excitation at 3 V_{PP}

Figure 6. *Laser Doppler interferometer measurements of the hub at two different actuation voltages.*

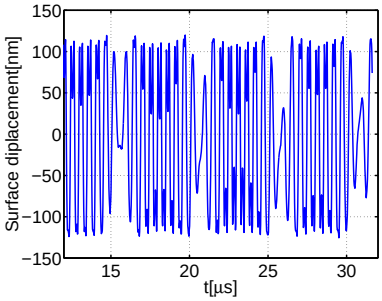

Figure 7. *Hub at 4 V_{PP} drive showing clipping due to rotor hub interaction. The rotor rotates continuously.*

$\omega = 2\pi \cdot 1.9$ MHz $h = 1$ μm, and $r_0 = 500$ μm giving $\dot{\theta}_{rotor} \approx 140/s$ or 1400 RPM. In practice, some sliding occurs between the rotor and stator that lowers the rotor velocity. In commercial bulk ultrasonic motors the rotor and stator are compressed to increase the friction and reduce sliding. Since the surface micromachined rotor and stator are not precompressed, substantial sliding can occur and the estimate from equation (2) should be considered a upper bound.

V. Motor Performance

Torque measurements

Measuring torque for micromotors is a challenge as the microgears cannot be directly interfaced with macro world instruments and because the output torque can be very small (often as small as $\sim 10^{-8}$N·m). Here the torque measurement was carried out with integrated serpentine springs with spring constant of 0.7mN/μm shown in Figure 8. By measuring the spring displacement in vacuum static torque of approximately 1 μN·m was obtained. During the torque measurements the spring broke off after 15-60 s of stressing although it is not clear whether

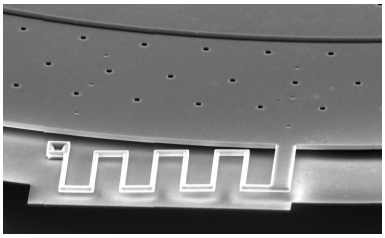

Figure 8. *SEM micrograph of one of the four serpentine springs attached to the rotor for torque measurement.*

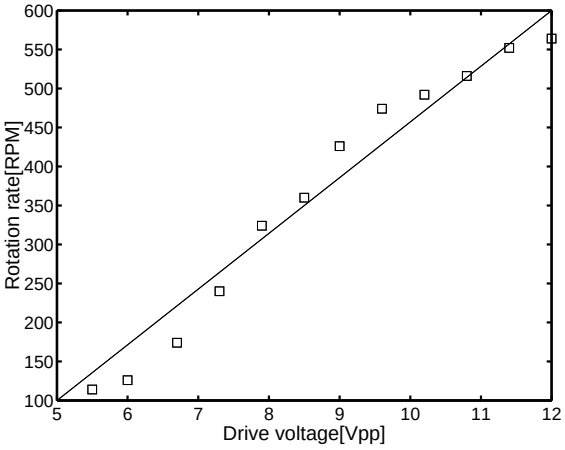

Figure 9. *RPM vs. drive voltage in vacuum*

Rotation in CW direction			
Rotation in CCW direction			

Figure 10. *Segmented electrode array drive configurations and resulting rotation direction. Solid boxes indicate the PZT segments that are enabled.*

this indicates high torque capability or if the breaking is due to combination of torque and ultrasonic fatigue.

RPM measurements

Figure 9 shows the rotation speed versus the drive voltage in vacuum. The rotation speed increases approximately linearly with the drive voltage. This is due to stronger contact between rotor and stator that increases friction between them. The measured motor velocity is smaller than estimated from the no-slip condition. Thus there is a velocity mismatch between the rotor and the stator that can result in frictional wear. In vacuum, the rotor stopped operating after three hours and wear induced particles were observed on the rotor near hub/rotor contact. In atmospheric pressure operation wear was not observed and the rotor was operated continuously for four days without failure but the RPM was an order of magnitude lower than in vacuum.

Rotation direction control

The rotation direction control is achieved by segmenting the PZT electrodes as shown in Figure 10. This dependency on the actuation point on rotation direction is due to phase difference between of the angular orientation of vibration modes and the excitation point.

VI. Conclusions

A surface micromachined ultrasonic rotor driven by a segmented PZT plate attached to the silicon substrate is demonstrated. It operates with a single-phase drive, which is different than the two or four phases needed for traditional ultrasonic motors. The nonlinear excitation of two neighboring modes leads to traveling waves that couple energy to the hub. The rotation direction is controlled by selective excitation of the PZT electrodes. High static torque capability (1 μN·m) was measured with integrated serpentine springs.

VII. Acknowledgments

We thank Wisconsin Center for Applied Microelectronics (WCAM) for technical support. We acknowledge Sandia National Laboratories for surface micromachine fabrication. We acknowledge National Science Foundation for funding.

References

[1] S. Ueha and Y. Tomikawa, *Ultrasonic Motors: Theory and Applications*, Clarendon Press, 1993.

[2] S. Hirose, Y. Yamayoshi, and H. Ono, "A Small Non-Contact Ultrasonic Motor", *IEEE Ultrasonic Symposium*, pp. 453–456, Baltimore, USA, Nov. 1993.

[3] R. Moroney, R. White, and R. H. R., "Ultrasonic Micromotors: Physics and Application", *IEEE Micro Electro Mechanical Systems*, pp. 182–187, Napa Valley, USA, Feb. 1990.

[4] A. Flynn, L. Tavrow, S. Bart, R. Brooks, D. Ehrlich, K. Udayakumar, and L. Cross, "Piezoelectric Micromotors for Microrobots", *IEEE Ultrasonics Symposium*, pp. 1163–1172, Honolulu, USA, 1990.

[5] V. Kaajakari, S. Rodgers, and A. Lal, "Ultrasonicly Driven Surface Micromachined Motor", *MEMS 2001*, pp. 40–45, Miyazaki, Japan, Jan. 23-2.57, 2000.

[6] M. S. Rodgers, J. J. Sniegowski, S. L. Miller, C. C. Barron, and P. J. McWhorter, "Advanced Micromechanisms in a Multi-Level Polysilicon Technology", *Proceedings of the SPIE*, pp. 120–130, Austin,TX, USA, Sep. 1997.

[7] G. Kino, *Acoustic Waves: Devices, Imaging, and Analog Signal Processing*, Prentice-Hall, 1987.

[8] H. W. Coover, Jr. and J. M. McIntire, *Handbook of Adhesives*, pp. 569–580, Van Nostrand Reinhold Company, 2nd ed., 1977.

[9] J. Zenneck, "Ueber die freien Schwingungen nur annähernd vollkommerer kreisförmiger Platten", *Annalen der Physik und Chemie*, vol. 67(2), pp. 165–184, Jan. 1899.

[10] M. Gèradin and D. Rixen, *Mechanical Vibrations: Theory and Applications to Structural Dynamics*, Wiley, 1994.